

Design of donor–acceptor type benzotri thiophene-based covalent organic frameworks for visible-light-driven overall water splitting

Cong Wang ^{a,1},, Diego Ontiveros ^{b,1},, Carmen Sousa ^{b,*},

^a School of Materials Science and Engineering, Changchun University of Science and Technology, Engineering Research Center of Optoelectronic Functional Materials, Ministry of Education, 130022, Changchun, China

^b Departament de Ciència de Materials i Química Física & Institut de Química Teòrica i Computacional (IQTCUB), Universitat de Barcelona, C/ Martí I Franquès 1-11, 08028, Barcelona, Spain

ARTICLE INFO

Keywords:

Photocatalysis
Overall water splitting
Covalent organic frameworks
Donor–acceptor photocatalysts
Density functional theory

ABSTRACT

Benefiting from the abundant accessible catalytic sites and well-defined porous architectures enhancing mass transport, two-dimensional (2D) covalent organic frameworks (COFs) are emerging as promising photocatalysts for overall water splitting (OWS). However, the performance of many known COFs for this application remains unsatisfactory, primarily due to stringent requirements for precise band alignment, the limitation posed by overpotentials in hydrogen evolution reaction (HER) and oxygen evolution reaction (OER), and mutual interference between the two half-reactions. Herein, we propose eight donor–acceptor (D–A) type 2D benzotri thiophene-based COFs (BTT-COFs), constructed from experimentally feasible building blocks via Schiff-base condensation reaction. By incorporating D–A pairs into the frameworks, these BTT-COFs exhibit enhanced intermolecular charge transfer characteristics as anticipated, thereby promoting efficient carrier separation during OWS. Concurrently, the D–A combinations enable precise modulation of the electronic structure, affording band gaps ranging from 2.35 to 2.89 eV with band-edge arrangements appropriately aligned for photocatalytic OWS under neutral conditions ($\text{pH} = 7$). Among them, the BTT-COF1 (incorporating benzotri thiophene and 1,3,5-triaminobenzene), BTT-COF2 (featuring benzotri thiophene and 2,4,6-triamino-1,3-diazine), and BTT-COF3 (consisting of benzotri thiophene and 2,4,6-triamino-1,3,5-triazine) are found to be capable of spontaneously driving OWS under their intrinsic photoinduced bias potentials. The remaining BTT-COFs require external bias to facilitate the reaction. Crucially, the theoretical solar-to-hydrogen (STH) conversion efficiencies of these materials range from 1.8 % to 10.0 %, highlighting their potential as efficient photocatalysts for OWS.

1. Introduction

With the accelerating global demand for energy, the pursuit of clean and renewable alternatives to fossil fuels has become increasingly urgent [1,2]. Hydrogen (H_2) is regarded as one of the most promising energy sources to tackle the global energy crisis on account of its high energy density and zero carbon emissions [3,4]. Among the various hydrogen production strategies, photocatalytic overall water splitting (OWS) stands out as a sustainable and cost-effective approach that directly converts solar energy into chemical fuel, offering a practical solution to global energy challenges while contributing to long-term carbon neutrality goals [5–8]. Photocatalytic OWS requires the

photocatalyst to meet two critical conditions: (i) a suitable band gap (1.23–3.10 eV) to harvest visible light efficiently, and (ii) proper band alignment, with the conduction band minimum (CBM) positioned above the H^+/H_2 reduction potential (-4.44 eV vs. vacuum) and the valence band maximum (VBM) positioned below the $\text{O}_2/\text{H}_2\text{O}$ half-reaction potential (-5.67 eV vs. vacuum) for $\text{pH} = 0$. In the past decades, a wide range of photocatalysts, ranging from inorganic to organic semiconductors, have been intensively investigated with the goal of achieving efficient energy conversion for water splitting [9–17]. However, their practical applications remain constrained by the high cost, limited visible-light utilization, low quantum efficiency stemming from recombination and trapping of light-induced carriers, and frequent

* Corresponding author.

E-mail address: c.sousa@ub.edu (C. Sousa).

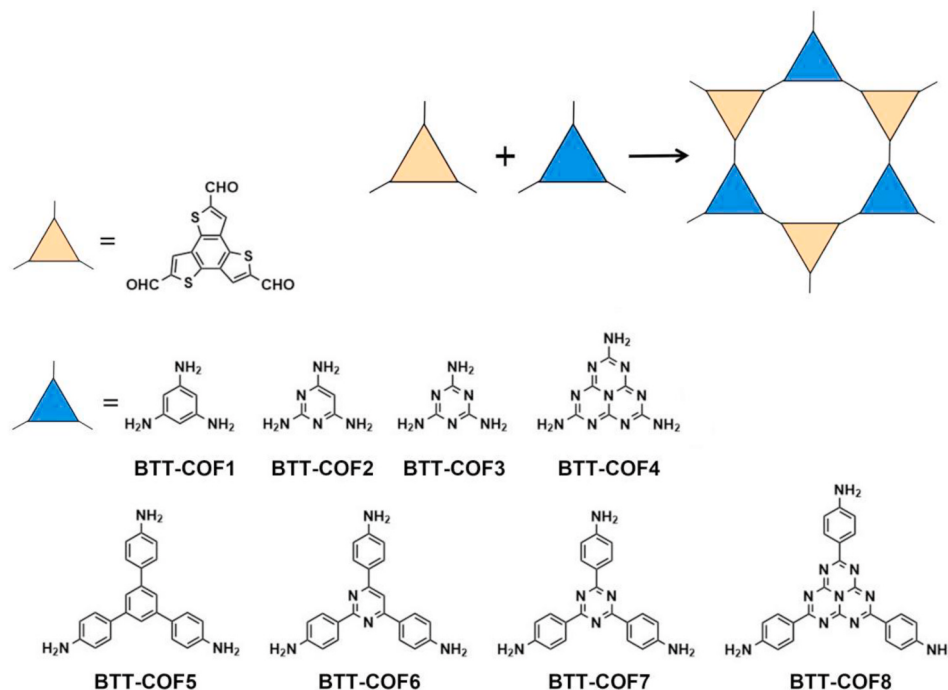
¹ These authors contributed equally.

reliance on sacrificial reagents or noble-metal-based cocatalysts. Hence, the rational design and development of novel, stable, and cost-effective photocatalysts capable of driving OWS in pure water remains a critical and urgent challenge.

Over the years, two-dimensional covalent organic frameworks (2D COFs), assembled from light-weight elements through robust covalent linkages, have emerged as a versatile class of photocatalytic materials for visible-light-driven OWS owing to their highly ordered crystalline structures, large surface area, tunable functionality, inherent porosity, and broad optical absorption capability [18,19]. Importantly, 2D COFs can be engineered at the molecular level by altering the functional monomers, enabling the specific design of photocatalysts tailored for efficient OWS [20,21]. To enhance the photoactivity of COFs for visible-light-driven OWS, various strategies have been explored, such as introducing specific functional groups [22,23], utilizing optimal donor–acceptor (D–A) combinations [24–31], or depositing suitable cocatalysts [32]. Among these strategies, constructing D–A type COFs, wherein electron-deficient and electron-rich moieties serve as acceptor and donor units, respectively, has emerged as a particularly attractive approach. The alternating arrangement of electron-deficient and electron-rich units in D–A COFs results in a spatially separated distribution of photogenerated electrons and holes, facilitating directional intermolecular charge migration from donor to acceptor moieties upon irradiation. Such dynamics enhance the efficient separation and transfer of photogenerated carriers, while effectively suppressing their recombination. Notably, while cocatalysts are often employed to further improve HER/OER rates in COF-based systems, several recent experimental studies have shown that pure COFs can exhibit photocatalytic activity without cocatalysts [33,34]. Motivated by these observations, the present work focuses on the intrinsic photocatalytic properties of the COFs themselves, aiming to explore their potential for OWS under visible-light irradiation. Moreover, by purposefully adjusting building blocks, the band gaps and band alignments of the COFs can be precisely tailored to meet specific photocatalytic requirements. In this regard, nitrogen-rich heterocyclic units such as diazine, triazine, and heptazine have attracted considerable attention as electron acceptors. These planar aromatic frameworks, composed of earth-abundant carbon and nitrogen atoms, exhibit strong electron affinity, favorable

photoexcitation characteristics, and excellent thermal and chemical stability, rendering them suitable active centers for hydrogen evolution reaction (HER) [35–41]. Conversely, sulfur-containing heterocycles, such as terthiophene-2,5,8-tricarboxaldehyde (commonly abbreviated as benzotri thiophene), demonstrate excellent hole transport properties and significant water oxidation activity [42–44], both of which are crucial for achieving OWS. Therefore, integrating intrinsically electron-deficient moieties such as diazine, triazine or heptazine as electron acceptors together with electron-rich aromatic structures like benzotri thiophene as donors within a single COF framework represents a promising molecular design strategy for high-performance photocatalytic systems. Further, the introduction of phenyl groups into these frameworks may exert a significant influence on their electronic structures and photocatalytic properties. Nevertheless, the detailed mechanisms underlying the photocatalytic performance of these D–A COFs, as well as their practical applications in OWS, remain insufficiently explored and deserve comprehensive investigation.

Herein, eight D–A type 2D benzotri thiophene-based covalent organic frameworks (BTT-COFs), as illustrated in **Scheme 1**, have been systematically developed via a topological design strategy, and their potential toward OWS has been comprehensively evaluated using first-principles computations by assessing their structural, electronic, optical, and photocatalytic properties. The present computational estimates indicate that all eight 2D frameworks are synthetically accessible and exhibit semiconducting characteristics with tunable band gaps spanning from 2.35 to 2.89 eV. Their band alignments all straddle the CBM and VBM at pH = 7, satisfying the thermodynamic requirements for OWS. Meanwhile, these BTT-COFs exhibit enhanced intermolecular charge transfer characteristics, thereby promoting efficient carrier separation during OWS. Among them, BTT-COF1 (constituted by benzotri thiophene as electron donor and 1,3,5-triaminobenzene as electron acceptor), BTT-COF2 (featuring benzotri thiophene and 2,4,6-triamino-1,3-diazine), and BTT-COF3 (alternating benzotri thiophene and 2,4,6-triamino-1,3,5-triazine units) are capable of spontaneously driving OWS under their intrinsic photoinduced bias potentials. The remaining BTT-COFs require external bias to facilitate the reaction. Notably, the theoretical solar-to-hydrogen (STH) conversion efficiencies of these materials range from 1.8 % to 10.0 %, underscoring their suitability and efficiency as



Scheme 1. Schematic diagram of the structural design principles of novel 2D BTT-COFs for photocatalytic overall water splitting.

photocatalysts for OWS.

2. Computational methods

All present density functional theory (DFT) calculations were performed by using the Vienna *ab initio* simulation package (VASP) [45], employing the Perdew-Burke-Ernzerhof (PBE) exchange-correlation functional within the generalized gradient approximation (GGA) [46, 47]. The core electron density has been described using the projector augmented wave (PAW) method [48], while valence electrons were described using an optimal planewave basis set with a kinetic energy cutoff of 415 eV. Convergence thresholds were set at 10^{-5} eV and 0.01 eV/Å for the energy and forces, respectively. To obtain accurate electronic structures, band alignments, and optical absorption spectra, the hybrid HSE06 functional was employed [49]. The Brillouin zone was sampled using an optimal Monkhorst-Pack mesh of $3 \times 3 \times 1$ dimensions [50]. A vacuum space of 15 Å was introduced along the *c*-axis to minimize interlayer interactions, as proven to be enough to fully isolate the 2D COFs [34, 51]. Dispersive forces were accounted using Grimme's D3 correction [52]. *Ab initio* molecular dynamics (AIMD) simulations were conducted to evaluate the thermodynamic stability of the proposed 2D BTT-COFs [53]. To assess the charge transfer, Bader charge analysis was performed [54]. The Gibbs free energy changes (ΔG) associated with the elementary steps of photocatalytic OWS were evaluated using the computational hydrogen electrode (CHE) model developed by Nørskov et al. [55]. Additional computational details can be found in the Supporting Information.

3. Results and discussion

3.1. Structure stability and experimental feasibility

To fabricate novel functionalized D–A type COFs for photocatalytic OWS, we employ a periodic design strategy that integrates the electron-rich benzotriophene unit with a series of electron-deficient linkers, including amino derivatives of benzene, diazine, triazine, heptazine, triphenylbenzene, triphenyldiazine, triphenyltriazine, and triphenylheptazine, within 2D networks. Applying this procedure, eight benzotriophene-based COFs, labeled as BTT-COFs (Scheme 1), have been constructed and their geometric structures fully optimized at the PBE level (see Figs. S1 and S2). The resulting lattice parameters vary from 14.46 to 24.19 Å, as summarized in Table 1, and are primarily dictated by the specific building blocks and linkages. Most BTT-COFs maintain planar configurations with zero torsion angles, except BTT-COF5, BTT-COF6, and BTT-COF7, which exhibit nonzero torsion angles due to intrinsic steric hindrance between central benzene, diazine or triazine rings and adjacent benzene rings. Specifically, BTT-COF5 and BTT-COF7 show torsion angles of 36.26° and 19.51°, respectively, while BTT-COF6 has two distinct torsion angles of 32.81° and 16.70° (Fig. S3). Interestingly, a clear trend is observed: as the nitrogen content in the central linker increases (from benzene to diazine, triazine, and heptazine), the torsion angles gradually decrease and the 2D framework

Table 1

Optimized lattice parameters, computed average reaction energy (E_r , eV) per stoichiometric formula, cohesive energy per atom (E_{coh} , eV), and formation energy per atom (E_f , eV) of 2D BTT-COFs ($c = 15$ Å, $\alpha = \beta = 90^\circ$, $\gamma = 120^\circ$).

BTT-COFs	$a = b$ (Å)	E_r	E_{coh}	E_f
BTT-COF1	14.70	−0.56	−5.82	−0.07
BTT-COF2	14.54	0.29	−5.85	−0.04
BTT-COF3	14.46	0.63	−5.87	−0.03
BTT-COF4	16.70	0.83	−5.93	−0.02
BTT-COF5	22.09	−1.18	−5.76	−0.12
BTT-COF6	21.89	−0.94	−5.77	−0.10
BTT-COF7	21.88	−0.81	−5.78	−0.10
BTT-COF8	24.19	−0.77	−5.83	−0.09

becomes more planar. Notably, BTT-COF8, constructed with a heptazine core, exhibits a completely planar structure. This highlights the critical role of N-rich linkers in modulating framework planarity and the concomitant electronic structures.

Experimentally, many 2D benzotriophene-based COFs have already been successfully synthesized [35, 39]. According to existing experimental findings, the assembly of benzotriophene units with linkers such as the ones studied here (amino derivatives of benzene, diazine, triazine, heptazine, triphenylbenzene, triphenyldiazine, triphenyltriazine, or triphenylheptazine) into 2D BTT-COFs is anticipated to be within reach via Schiff-base condensation reaction. Here, we propose possible synthetic routes for all eight 2D BTT-COFs and compute their corresponding average reaction energy (E_r) per stoichiometric formula to assess their experimental feasibility (Figs. S4 and S5, Table 1), as done in Refs 20, 35, 38. The computed E_r values from BTT-COF1 to BTT-COF8 are −0.56, 0.29, 0.63, 0.83, −1.18, −0.94, −0.81, and −0.77, respectively. From a thermodynamic perspective, most of the reactions are exothermic. Although the synthesis of BTT-COF2, BTT-COF3, and BTT-COF4 are endothermic processes, their formation remains feasible under elevated reaction temperatures. To further assess structural stability, we calculate the cohesive (E_{coh}) and formation (E_f) energies per atom. All BTT-COFs exhibit E_{coh} values below −5.00 eV and negative E_f values, which are comparable to those of previously reported synthesized 2D COFs, such as PTEB [51, 56], and CHF-1 [38], highlighting their strong structural robustness and favorable bonding formation. Additionally, the thermal stability of these materials is validated through AIMD simulations (Figs. S6–S13). After 5 ps simulations, these structures emerge with some minor distortions relative to the original configurations; however, the overall 2D frameworks remain well-preserved, with no bond breakage observed, thereby confirming the reliable thermal stability of the BTT-COFs. Based on these results, we foresee that all eight BTT-COFs studied are synthetically accessible. Indeed, the BTT-COF5 and BTT-COF7 have already been successfully synthesized, providing experimental support for our computational study.

3.2. Band alignment

After validating the experimental feasibility of these 2D BTT-COFs, we systematically explore their electronic structures to evaluate their potential as photocatalysts for OWS under visible-light irradiation at pH = 7. To this end, we first calculate their band structures using the hybrid HSE06 functional, as photocatalytic performance is primarily governed by two key factors: (i) an appropriate band gap (typically 1.23–3.10 eV) for efficient visible-light absorption, and (ii) suitable band alignments, with the conduction band minimum (CBM) located above the H^+/H_2 redox potential (−4.44 eV vs. vacuum) and the valence band maximum (VBM) situated below the O_2/H_2O potential (−5.67 eV vs. vacuum) for pH = 0. As shown in Figs. 1 and 2, and Table S1, all BTT-COFs exhibit

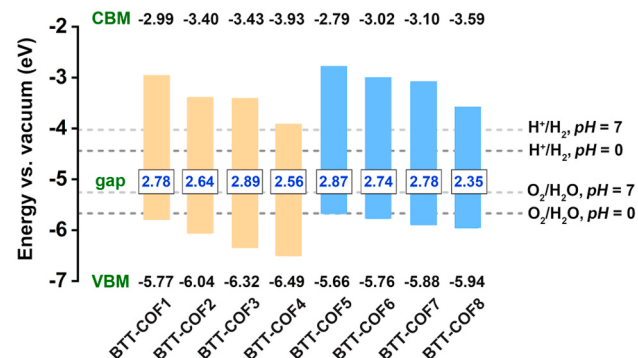


Fig. 1. Band alignment diagram for the eight 2D BTT-COFs relative to the vacuum level. Horizontal dashed lines represent the redox potential energy levels of the half-reactions of water splitting at pH = 0 and pH = 7.

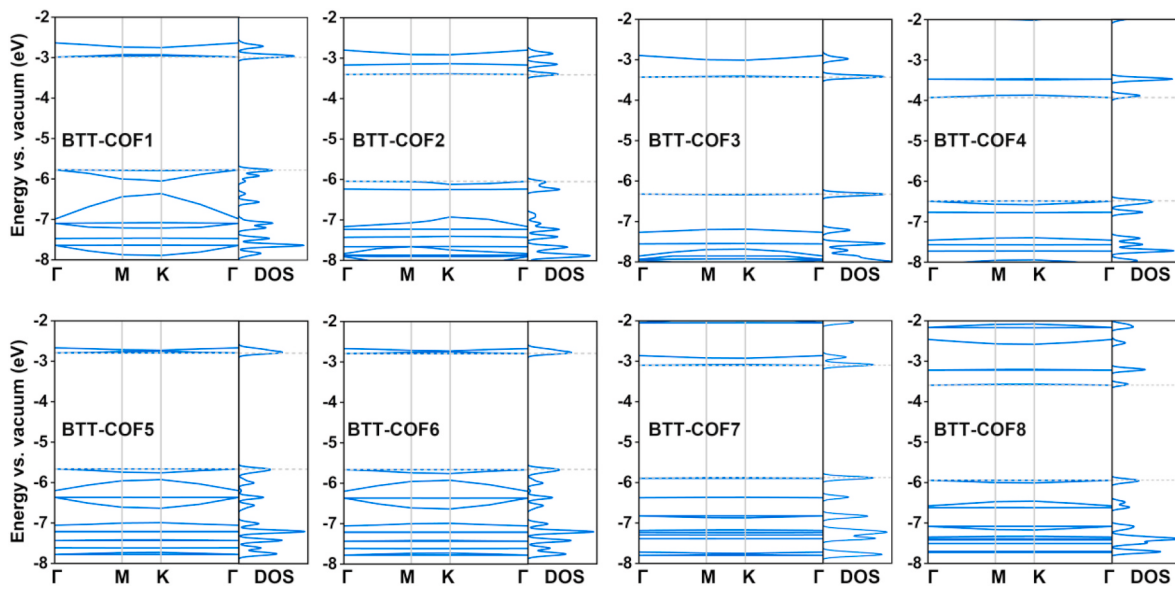


Fig. 2. Computed HSE06 electronic band structures and density of states (DOS) relative to vacuum level of BTT-COFs.

semiconducting behavior with band gaps ranging from 2.35 to 2.89 eV. Unlike graphene, these BTT-COFs exhibit flat bands near the Fermi level. As mentioned above, these frameworks can be synthesized via Schiff-base condensation reaction, in which the building blocks are connected through C=N bonds. This bonding scheme may localize the conjugated π electrons, contributing to the emergence of unusual flat bands at both the CBM and VBM [20]. Importantly, their CBM and VBM positions straddle the water redox potentials at pH = 7, which meets the thermodynamic requirements for OWS, thereby positioning them as promising candidates for photocatalytic OWS. Moreover, a clear trend is observed from BTT-COF1 to BTT-COF4: as the N content in the linkers increases, both the CBM and VBM systematically shift downward. A similar pattern is also apparent across the BTT-COF5 to BTT-COF8 series, indicating that N-rich linkers tend to lower the energy levels of the frontier orbitals, likely due to their electron-withdrawing nature. Conversely, when comparing BTT-COF1 and BTT-COF5, BTT-COF2 and BTT-COF6, BTT-COF3 and BTT-COF7, and BTT-COF4 and BTT-COF8, the incorporation of additional benzene rings in BTT-COF5, BTT-COF6, BTT-COF7, and BTT-COF8 increases the overall carbon content and π -conjugation, hence resulting in an obvious upward shift of both CBM and VBM. These contrasting behaviors imply that introducing N-rich linkers is more favorable for OER by lowering the VBM, while C-rich, π -conjugated linkers are more advantageous for HER by elevating the CBM. This structure-property relationship provides a strategic guideline for the rational design of COFs with finely tuned band alignments to enhance their photocatalytic performance for OWS.

3.3. Charge carriers separation

To explore the charge carrier separation behavior of these materials, which is critical for minimizing electron-hole recombination and enhancing photocatalytic efficiency, we first examine the charge density distributions of the CBM and VBM by both qualitative and quantitative analyses. As visualized in Fig. S14, a qualitative assessment reveals that in BTT-COF1, BTT-COF3, BTT-COF5, and BTT-COF7, the charge densities of the CBM and VBM are relatively delocalized across the entire framework, indicating moderate charge separation. In contrast, BTT-COF2 and the benzene-containing counterpart BTT-COF6 exhibit markedly improved spatial separation between CBM and VBM. This improvement can be attributed to the presence of diazine and triphenyldiazine linkers, which effectively reduce the symmetry of the frameworks and thus facilitate charge separation. Likewise, in BTT-

COF4 and BTT-COF8, the CBM is primarily localized on the heptazine or triphenylheptazine units, whereas the VBM is predominantly distributed over the benzotriphosphine moieties, also suggesting strong spatial separation of frontier orbitals. To complement these observations, a quantitative analysis is conducted by computing the spatial overlap integral between the charge densities of the CBM and VBM [57]. This metric, presented in Fig. 3 and summarized in Table S2, provides a rigorous measure of the extent of charge separation (see SI). The results confirm that BTT-COF2, BTT-COF4, BTT-COF6, and BTT-COF8 exhibit significantly lower CBM-VBM overlap values compared to the other BTT-COFs, reinforcing their potential to minimize electron-hole recombination and enhance photocatalytic performance. In addition, Bader charge analysis was conducted to gain deeper insights into the nature of the interfragment charge transfer within the frameworks. The results indicate that all eight BTT-COF systems exhibit pronounced D-A characteristics (see Table S2). As expected, building blocks, such as benzene, diazine, triazine, heptazine, triphenylbenzene, triphenyldiazine, triphenyltriazine, and triphenylheptazine, act as electron acceptors, drawing electrons from the benzotriphosphine moieties. The total amounts of interfragment charge transfer in the eight BTT-COF systems were quantified to be 2.16, 2.40, 2.46, 2.47, 2.12, 2.20, 2.34, and 2.22 $|e|$, respectively. The noticeable charge transfer observed among these frameworks confirms the D-A character of the COFs, thus enhancing their feasibility to be excellent candidates toward photocatalytic OWS.

Generally, a photoinduced electron–hole pair typically persists for an average lifetime before undergoing recombination. To achieve high photocatalytic efficiency, it is crucial to prolong this lifetime by promoting effective spatial separation of charge carriers. The efficiency of this separation is primarily determined by the relative mobilities of the generated electrons and holes. As such, semiconductors with strongly unbalanced carrier mobilities tend to suppress rapid recombination and thereby exhibit longer carrier lifetimes. Given the inverse relationship between carrier mobility and effective mass (eq. (8) of the SI), we initially evaluate the effective masses of photogenerated electrons (m_e^*) and holes (m_h^*) along two perpendicular directions, x and y , which correspond to the zigzag and armchair directions. This analysis provides preliminary insights into the degree of charge separation within the material. As summed in Table S3, BTT-COF2 stands out among the evaluated candidates, exhibiting notable anisotropy and disparity between m_e^* and m_h^* , which are beneficial for promoting charge separation and prolonging carrier lifetimes. By contrast, BTT-COF4 displays nearly

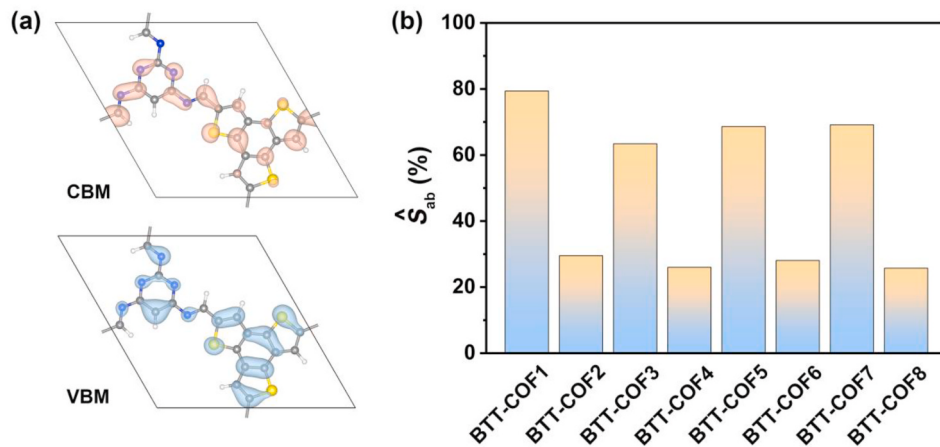


Fig. 3. (a) CBM (orange) and VBM (blue) partial charge densities of the 2D BTT-COFs, at an isovalue of $0.002 \text{ e}\cdot\text{\AA}^{-3}$. (b) Spatial overlap, \hat{S}_{ab} , percentage between the CBM and VBM charge densities for these 2D BTT-COFs. (For interpretation of the references to colour in this figure legend, the reader is referred to the Web version of this article.)

isotropic effective masses for both carriers along the x and y directions. While the m_e^* are relatively small (~ 1.60 and $1.42 m_0$ along x and y directions, respectively), the m_h^* are remarkably large ($\sim 26 m_0$), significantly restricting hole mobility and hindering balanced charge transport. Other candidates, including BTT-COF1, BTT-COF3, and BTT-COF6, possess nearly balanced m_e^* and m_h^* , generally unfavorable for effective charge separation. In the case of BTT-COF5, the VB near the Fermi level is nearly flat, making direct extraction of the m_h^* impractical; the value is therefore estimated using the second-lowest valence band ($\sim 0.80 m_0$). Similarly, BTT-COF7 exhibits extremely heavy m_e^* , exceeding $90 m_0$, while BTT-COF8 also features a flat VB, with its m_h^* taken from the second-lowest band ($\sim 0.68 m_0$). Despite their pronounced electron–hole mobility imbalance, both BTT-COF7 and BTT-COF8 display isotropic electron transport behavior, analogous to that of BTT-COF4.

Following the above analyses of charge separation and effective masses, BTT-COF2 and BTT-COF4 are selected for carrier mobility (μ) calculations (see SI) to gain deeper insight into their charge transport behavior based on the deformation potential (DP) theory [58]. All key parameters, including effective masses (m^*), deformation potential constant (E_d), elastic modulus (C_{2D}), and the corresponding μ are summarized in Figs. S15–S16 and Tables S4–S5. The results, also visualized in Fig. 4, reveal that BTT-COF2 exhibits a unique type of anisotropic behavior. Along the x direction, both electrons and holes possess higher mobilities, with hole mobility being nearly twice that of electrons. In

contrast, along the y direction, the trend is reversed, with electrons exhibiting greater mobility than holes. The disparity within each direction promotes the spatial charge separation, thereby diminishing electron–hole recombination, prolonging carrier lifetimes, and ultimately enhancing photocatalytic performance. Conversely, BTT-COF4 consistently favors electron transport in both directions, and also presents disparity with respect to the holes, but suffers from extremely poor hole mobility and lacks directional preference, which may lead to charge accumulation and elevated recombination probability, ultimately limiting its photocatalytic efficiency.

3.4. Optical absorption

Photoconversion efficiency is a key metric for photocatalysts, and it strongly depends on their light-harvesting capabilities [59]. To simply illustrate the light-harvesting abilities of the BTT-COFs, their optical absorption spectra have been calculated, as efficient utilization of solar energy is vital for photocatalytic applications. As shown in Fig. 5, all BTT-COFs demonstrate pronounced absorption in the visible-light region, with absorption coefficients (α) reaching up to 10^5 cm^{-1} . Notably, this computational prediction is strongly supported by experimental data for the synthesized analogs, BTT-COF5 and BTT-COF7, which also show significant visible-light absorption [60]. Concurrently, all of them, including both the predicted and experimentally reported structures, exhibit distinct absorption peaks within the visible-light region,

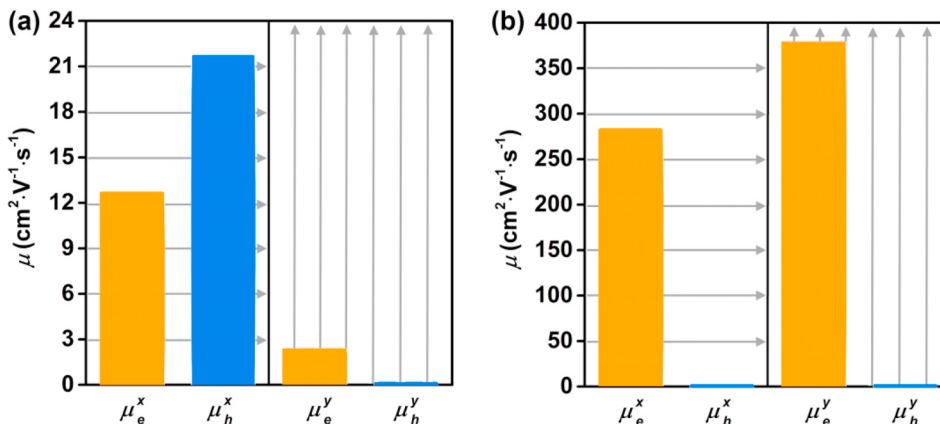


Fig. 4. Charge carrier mobility, μ , $\text{cm}^2 \cdot \text{V}^{-1} \cdot \text{s}^{-1}$, for the electrons and holes along the x and y directions for (a) BTT-COF2 and (b) BTT-COF4. The orange and blue bars indicate the electron and hole mobilities, respectively. (For interpretation of the references to colour in this figure legend, the reader is referred to the Web version of this article.)

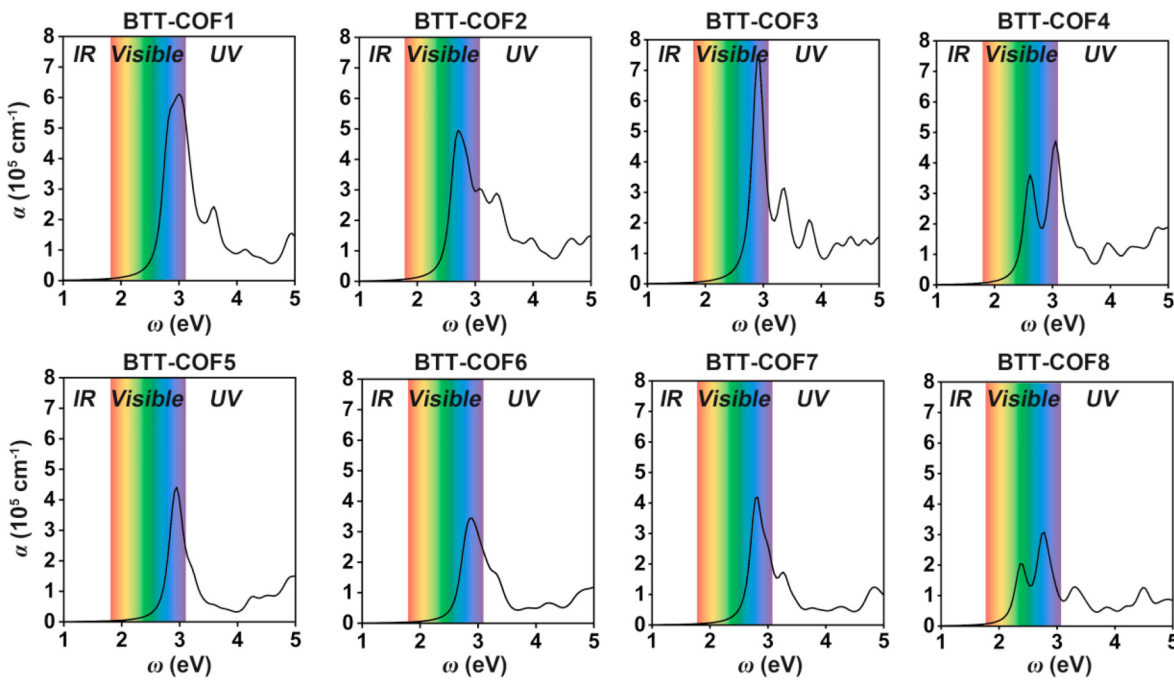


Fig. 5. Optical absorption spectra of the 2D BTT-COFs at the HSE06 level.

confirming their capability for electronic excitation under solar irradiation. This highlights their superior light-harvesting capabilities and underscores their potential as promising candidates for visible-light-responsive photocatalysts.

3.5. Solar-driven overall water splitting

To achieve the OWS on 2D BTT-COFs under visible-light irradiation, it is essential that the photoinduced potentials, namely, the irradiation-induced electron (U_e) and hole (U_h) potentials (Table S1), must possess sufficient energy to simultaneously drive the hydrogen evolution

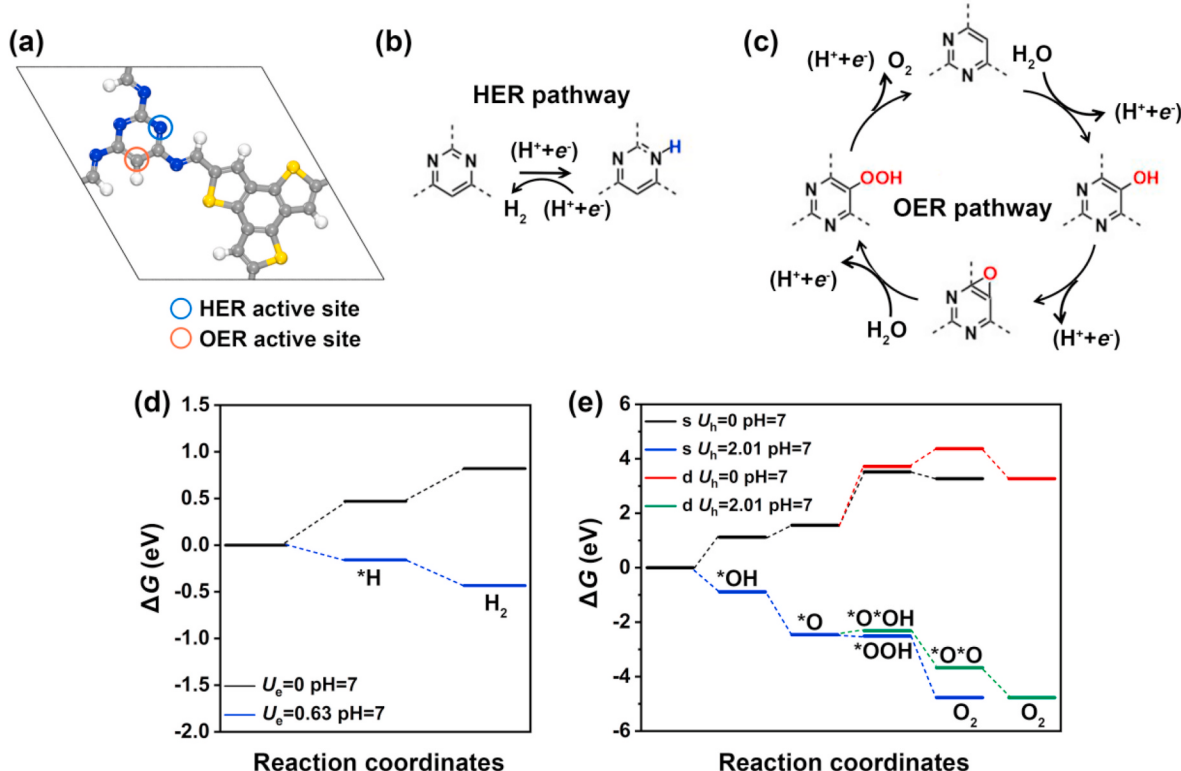


Fig. 6. (a) Ball-stick model for the unit cell of BTT-COF2 and its optimal active sites for water splitting, where the blue and red circles represent the HER and single-site/dual-site OER active sites, respectively. Preferred reaction pathways of the (b) HER and (c) OER on BTT-COF2. Gibbs free energy profiles of (d) HER and (e) OER of BTT-COF2. (For interpretation of the references to colour in this figure legend, the reader is referred to the Web version of this article.)

reaction (HER) and oxygen evolution reaction (OER) [20]. Otherwise, external inputs such as sacrificial agents, cocatalysts, or applied bias would be required. Here, the Gibbs free energy changes (ΔG) of intermediate states involved in HER and OER processes have been computed to verify whether the irradiation-induced carriers could drive the redox reaction of water (see computational details in the Supporting Information).

The HER activity of all 2D BTT-COFs was initially investigated via the classical $2e^-$ reaction pathway ($2H^+ + 2e^- \rightarrow H_2$). To determine the most favorable catalytic sites, the Gibbs free energy variation for the first step of HER, ΔG_{*H} , was calculated for all inequivalent reaction sites at pH = 7, and the results are summarized in Tables S6–S13. The data show that the optimal HER active sites for all systems are located on N atoms within these frameworks. Subsequently, the Gibbs free energy profiles of HER processes on these BTT-COFs, both in the absence and presence of the light-induced potential U_e , were plotted and are illustrated in Fig. 6 for BTT-COF2 and in Figs. S17–S23 for the rest of the BTT-COFs. The results reveal that, under visible-light irradiation, BTT-COF1, BTT-COF2, BTT-COF3, BTT-COF5, BTT-COF6, and BTT-COF7 exhibit spontaneous HER activity, leaving only the exceptions of BTT-COF4 and BTT-COF8, which show no spontaneous HER activity at any reactive site under illumination. The lack of photocatalytic HER activity in these two frameworks can be attributed to their relatively high N content, which significantly lowers the CBM, thereby reducing the thermodynamic driving force for proton reduction.

Following the HER evaluation, the OER performance of all 2D BTT-COFs was analyzed based on the conventional $4e^-$ reaction pathway ($2H_2O \rightarrow O_2 + 4H^+ + 4e^-$). This multistep process involves a sequence of intermediates, including $*OH$, $*O$, $*OOH/*O*OH$, and $*OO$ species. According to previous studies, two mechanisms may operate on such frameworks: the single-site (s) and dual-site (d) pathways [20,33,38]. Both mechanisms begin with water dissociation to form $*OH$ ($* + H_2O \rightarrow *OH + H^+ + e^-$), followed by $*OH$ oxidation to $*O$ ($*OH \rightarrow *O + H^+ + e^-$). The divergence arises in the third step: the single-site mechanism proceeds via nucleophilic attack by another water molecule to form $*OOH$ ($*O + H_2O \rightarrow *OOH + H^+ + e^-$), whereas the dual-site mechanism involves the coadsorption of $*O$ and $*OH$ to produce $*O*OH$ ($*O + H_2O \rightarrow *O*OH + H^+ + e^-$). The O_2 evolution is completed by $*OOH$ decomposition ($*OOH \rightarrow * + O_2 + H^+ + e^-$) in the single-site case, or $*O*OH$ oxidation to $*O*O$ followed by desorption ($*O*OH \rightarrow *O*O + H^+ + e^-$; $*O*O \rightarrow * + O_2$) in the dual-site case. Similar to HER analysis, the Gibbs free energy variation for the first step of OER, ΔG_{*OH} , was evaluated at pH = 7 across all inequivalent reaction sites to identify the most favorable catalytic centers. The detailed data are provided in Tables S6–S13. Subsequently, the Gibbs free energy profiles for the OER were depicted for each BTT-COF, both in the absence and presence of the light-induced potential U_h (Fig. 6 and S17–S23). Without light-induced bias, all OER steps exhibit uphill energy profiles, indicating inherent thermodynamic limitations. However, upon application of U_h , the ΔG values for each step in BTT-COF1, BTT-COF2, BTT-COF3, and BTT-COF4 shift to negative values, implying that photogenerated holes could provide sufficient driving force to enable spontaneous oxygen evolution. Specifically, OER occurs on benzene and diazine rings in BTT-COF1 and BTT-COF2, respectively, whereas in BTT-COF3 and BTT-COF4, it takes place on the benzotri thiophene moiety. This observation suggests that in D–A COFs, the optimal OER active sites are not necessarily confined to the donor moieties; instead, they may be determined by the local electronic environment and the binding strength toward reaction intermediates, leading to distinct site preferences across different frameworks. Hence, the BTT units act primarily as photoactive donor moieties, modulating directional charge separation, enhancing visible-light absorption through strong π -conjugation and facilitating intralayer charge transport, boosting the photocatalytic activity of the D–A COFs. Besides, with the exception of BTT-COF2, the dual-site mechanism is found to be more favorable than the single-site pathway. In contrast, BTT-COF5, BTT-COF6, BTT-COF7, and

BTT-COF8 show no spontaneous OER activity under illumination. This poor OER performance can be attributed to their relatively high C content, which significantly raises the VBM, thereby decreasing the thermodynamic driving force required for water oxidation. Integrating these HER and OER results, BTT-COF1, BTT-COF2, and BTT-COF3 are identified as the most promising candidates for OWS. Their HER and OER free energy profiles consistently show downhill trends under visible-light irradiation at pH = 7, confirming their intrinsic ability to drive spontaneous OWS without the need for sacrificial agents, co-catalysts, or external bias. Nevertheless, under photoelectrocatalytic conditions, where an external bias potential is applied, BTT-COF4–8 also demonstrate the ability to efficiently drive the OWS, as shown in Figs. S19–S23.

Finally, to evaluate the practical applicability of these 2D materials for solar-driven OWS, we calculate their solar-to-hydrogen (STH) conversion efficiencies under neutral conditions (pH = 7) [61], as summarized in Table 2. The results reveal a pronounced inverse correlation between the optical absorption efficiency and the band gap, where larger band gaps are generally associated with diminished light-harvesting capabilities and lower carrier utilization. The estimated STH efficiencies span from 1.8 % to 10.0 %, thereby reinforcing the potential of these BTT-based COFs as candidates for visible-light-driven OWS applications.

4. Conclusions

To summarize, we develop eight D–A type 2D BTT-COFs and systematically explore their potential as photocatalysts for water splitting. The present computational estimates indicate that all eight 2D frameworks are synthetically accessible, confirmed by the calculation of reaction, cohesive, and formation energies, and AIMD simulations. By incorporating D–A pairs into the frameworks, their band gaps can be well tuned with the values spanning from 2.35 to 2.89 eV, which falls within the visible-light range, making them suitable for photocatalysis. Moreover, their band alignments all straddle the CBM and VBM at pH = 7, satisfying the thermodynamic requirements for OWS. Bader charge analysis reveals significant intermolecular charge transfer (2.12–2.47 | e|) from donor to acceptor segments within these 2D BTT-COFs, helping to promote efficient carrier separation during OWS. Among them, the BTT-COF1 (composed by benzotri thiophene and benzene units), BTT-COF2 (featuring benzotri thiophene and diazine), and BTT-COF3 (consisting of benzotri thiophene and triazine) can spontaneously photocatalyze OWS under their intrinsic photoinduced bias potentials. The remaining BTT-COFs require external bias to facilitate the reaction. Additionally, a unique type of anisotropic behavior has been observed for BTT-COF2, wherein both electrons and holes demonstrate relatively high mobilities along the x direction, however, the hole mobility significantly surpasses that of the electrons. Conversely, along the y direction, this trend is reversed, with electrons showing higher mobilities than holes. These disparity and complementary migration trends significantly promote the separation of charge carriers, thereby

Table 2

Parameters for the STH efficiency estimate, χ_{H_2} and χ_{O_2} being the HER and OER overpotentials at pH = 7, respectively, all given in eV, and η_{abs} , η_{cu} , and η_{STH} representing the efficiency of light absorption, carrier utilization, and STH, respectively, given in percentage.

BTT-COFs	χ_{H_2}	χ_{O_2}	η_{abs}	η_{cu}	η_{STH}
BTT-COF1	1.04	0.51	10.1	31.9	3.2
BTT-COF2	0.63	0.78	13.7	40.9	5.6
BTT-COF3	0.60	1.06	8.1	38.3	3.1
BTT-COF4	0.10	1.23	16.1	33.6	5.4
BTT-COF5	1.24	0.40	8.4	21.6	1.8
BTT-COF6	1.01	0.50	11.1	30.8	3.4
BTT-COF7	0.93	0.62	10.1	39.3	4.0
BTT-COF8	0.44	0.68	22.7	44.3	10.0

minimizing electron–hole recombination and improving the overall efficiency of photocatalytic OWS. Crucially, the theoretical STH conversion efficiencies of these materials range from 1.8 % to 10.0 %, highlighting their superior photocatalytic performance. Overall, all the D–A COFs proposed in this work satisfy the thermodynamic requirements for OWS, although certain systems may necessitate the application of an external bias. Beyond providing a deeper understanding of structure–property relationships and guiding the rational design of efficient D–A COF photocatalysts, the intrinsic features of these frameworks open exciting opportunities for a broader range of light-triggered applications, including CO_2 photoreduction, nitrogen fixation, and organic pollutant degradation. These findings lay a solid foundation for the future development of multifunctional COF-based photocatalysts with tailored electronic and structural properties.

CRediT authorship contribution statement

Cong Wang: Writing – original draft, Methodology, Investigation, Formal analysis, Conceptualization. **Diego Ontiveros:** Writing – review & editing, Methodology, Formal analysis. **Carmen Sousa:** Writing – review & editing, Supervision, Resources, Funding acquisition.

Declaration of competing interest

The authors declare that they have no known competing financial interests or personal relationships that could have appeared to influence the work reported in this paper.

Acknowledgements

The authors acknowledge financial support from the Spanish *Ministerio de Ciencia e Innovación* and *Agencia Estatal de Investigación* (AEI) MCIN/AEI/10.13039/501100011033 through grants PID2021-126076NB-I00 and PID2024-159906NB-I00, the unit of excellence *María de Maeztu* CEX2021-001202-M granted to the IQTCUB, and the *Generalitat de Catalunya* 2021SGR00079 grant. C.W. acknowledges financial support from the National Natural Science Foundation of China (22401018), the Science and Technology Development Plan of Jilin Province of China (20220508029RC), the Education Department of Jilin Province of China (JJKH20240928KJ and JJKH20220758KJ), and the China Scholarship Council (CSC, 202307580027). D.O. thanks *Universitat de Barcelona* for a predoctoral contract (PREDOCS-UB).

Appendix B. Supplementary data

Supplementary data to this article can be found online at <https://doi.org/10.1016/j.ijhydene.2025.153153>.

References

- [1] Lewis NS. Toward cost-effective solar energy use. *Science* 2007;315:798–801.
- [2] Larcher D, Tarascon JM. Towards greener and more sustainable batteries for electrical energy storage. *Nat Chem* 2015;7:19–29.
- [3] Turner JA. Sustainable hydrogen production. *Science* 2004;305:972–4.
- [4] Squadrato G, Maggio G, Nicita A. The green hydrogen revolution. *Renew Energy* 2023;216:119041.
- [5] Maeda K, Domen K. Photocatalytic water splitting: recent progress and future challenges. *J Phys Chem Lett* 2010;1:2655–61.
- [6] Hisatomi T, Domen K. Reaction systems for solar hydrogen production via water splitting with particulate semiconductor photocatalysts. *Nat Catal* 2019;2:387–99.
- [7] Ontiveros D, Vela S, Viñes F, Sousa C. MXgap: a MXene learning tool for bandgap prediction. *ACS Catal* 2025;15:14403–13.
- [8] Bie C, Wang L, Yu J. Challenges for photocatalytic overall water splitting. *Chem* 2022;8:1567–74.
- [9] Formal FL, Pendlebury SR, Cornuz M, Tilley SD, Grätzel M, Durrant JR. Back electron-hole recombination in hematite photoanodes for water splitting. *J Am Chem Soc* 2014;136:2564–74.
- [10] Chen X, Shen S, Guo L, Mao SS. Semiconductor-based photocatalytic hydrogen generation. *Chem Rev* 2010;110:6503–70.
- [11] Zhang X, Zhang Z, Wu D, Zhang X, Zhao X, Zhou Z. Computational screening of 2D materials and rational design of heterojunctions for water splitting photocatalysts. *Small Methods* 2018;2:1700359.
- [12] Liu X, Zhang Y, Wang C, Shen L. Polar materials for photocatalytic applications: a critical review. *Interdiscip Mater* 2024;3:530–64.
- [13] Jian S, Xiao Q, Huang J, Ye J, Zhang L, Xu L, Xie Q. A highly efficient $\text{Bi}_2\text{O}_3\text{Se}/\text{Bi}_2\text{WO}_6$ S-Scheme heterojunction photocatalyst for solar water splitting: a first-principles study. *Langmuir* 2025;41:23761–71.
- [14] Ontiveros D, Viñes F, Sousa C. Bandgap engineering of MXene compounds for water splitting. *J Mater Chem A* 2023;11:13754–64.
- [15] Jia X, Wang C, Li Y, Zhang R, Shi Z, Liu X, Yu X, Zhang M, Xing Y. All-solid-state Z-scheme $\text{Ta}_3\text{N}_5/\text{Bi/CaTaO}_2\text{N}$ photocatalyst transformed from perovskite $\text{CaBi}_2\text{Ta}_2\text{O}_9$ for efficient overall water splitting. *Chem Eng J* 2022;431:134041.
- [16] Mao D, Wan R, Zhang Z, Li M, Tian G, Chen S. First-principles investigation of monolayer $\text{Sc}_2\text{Se}_2\text{X}_2$ ($X = \text{Cl}, \text{Br}$) as a high-performance photocatalyst for efficient water splitting. *Langmuir* 2025;41:8822–33.
- [17] Ontiveros D, Vela S, Vines F, Sousa C. Tuning MXenes towards their use in photocatalytic water splitting. *Energy Environ Mater* 2024;7:e12774.
- [18] Ding SY, Wang W. Covalent organic frameworks (COFs): from design to applications. *Chem Soc Rev* 2013;42:548–68.
- [19] Feng X, Ding X, Jiang D. Covalent organic frameworks. *Chem Soc Rev* 2012;41:6010–22.
- [20] Wan Y, Wang L, Xu H, Wu X, Yang J. A simple molecular design strategy for two-dimensional covalent organic framework capable of visible-light-driven water splitting. *J Am Chem Soc* 2020;142:4508–16.
- [21] Sheng L, Wang W, Wang J, Zhang W, Li Q, Yang J. Data-driven discovery of a covalent organic framework heterojunction as efficient photocatalysts for overall solar water splitting. *J Phys Chem Lett* 2024;15:5016–23.
- [22] Xia X, Feng J, Zhong Z, Yang X, Li N, Chen D, Li Y, Xu Q, Lu J. Reconstruction of D-II-A polymer accelerating photocatalytic degradation of BPA and production of H_2O_2 . *Adv Funct Mater* 2024;34:2311987.
- [23] Gu YY, Wang J, Tang Q, Wei H, Ning J, Lan X, Wang X, Li X, Jia Y, Wang S, Hao L. Insights into substituent effects on the fundamental photocatalytic processes of covalent organic frameworks toward H_2 evolution and H_2O_2 production reactions. *ACS Catal* 2024;14:11262–72.
- [24] Li Z, Zhang Z, Nie R, Li C, Sun Q, Shi W, Chu W, Long Y, Li H, Liu X. Construction of stable donor–acceptor type covalent organic frameworks as functional platform for effective perovskite solar cell enhancement. *Adv Funct Mater* 2022;32:2112553.
- [25] Ghosh S, Nakada A, Springer MA, Kawaguchi T, Suzuki K, Kaji H, Baburin I, Kuc A, Heine T, Suzuki H, Abe R, Seki S. Identification of prime factors to maximize the photocatalytic hydrogen evolution of covalent organic frameworks. *J Am Chem Soc* 2020;142:9752–62.
- [26] Wang L, Liu L, Li Y, Xu Y, Nie W, Cheng Z, Zhou Q, Wang L, Fan Z. Molecular-level regulation strategies toward efficient charge separation in donor–acceptor type conjugated polymers for boosted energy-related photocatalysis. *Adv Energy Mater* 2024;14:2303346.
- [27] Qian Y, Han Y, Zhang X, Yang G, Zhang G, Jiang HL. Computation-based regulation of excitonic effects in donor–acceptor covalent organic frameworks for enhanced photocatalysis. *Nat Commun* 2023;14:3083.
- [28] Ren H, Zhao X, Lang Z, Tan H, Wang Y, Li Y. β -Ketoenamine linkage-engineered donor–acceptor covalent heptazine polymers for efficient visible-light-driven overall water splitting. *Chem Eng J* 2025;526:170975.
- [29] Sheng L, Wang W, Wang J, Zhang W, Li Q, Yang J. High-throughput computational screening of novel two-dimensional covalent organic frameworks for efficient photocatalytic overall water splitting. *J Phys Chem Lett* 2024;15:5016–23.
- [30] Li R, Du J, Zhou T, Huang T. Rational design of effective photocatalysts for water splitting by assembling a donor and an acceptor into covalent organic frameworks. *J Phys Chem C* 2025;129:10009–19.
- [31] Xia Y, Zhang W, Yang S, Wang L, Yu G. Research progress in donor–acceptor type covalent organic frameworks. *Adv Mater* 2023;35:2301190.
- [32] Yang S, Hu W, Zhang X, He P, Pattengale B, Liu C, Cendejas M, Hermans I, Zhang X, Zhang J, Huang J. 2D covalent organic frameworks as intrinsic photocatalysts for visible light-driven CO_2 reduction. *J Am Chem Soc* 2018;140:14614–8.
- [33] Du X, Ji H, Xu Y, Du S, Feng Z, Dong B, Wang R, Zhang F. Covalent organic framework without cocatalyst loading for efficient photocatalytic sacrificial hydrogen production from water. *Nat Commun* 2025;16:3024.
- [34] Shen R, Qin C, Hao L, Li X, Zhang P, Li X. Realizing photocatalytic overall water splitting by modulating the thickness-induced reaction energy barrier of fluorenone-based covalent organic frameworks. *Adv Mater* 2023;35:2305397.
- [35] Zhao Y, Wang C, Han X, Lang Z, Zhao C, Yin L, Sun H, Yan L, Ren H, Tan H. Two-dimensional covalent heptazine-based framework enables highly photocatalytic performance for overall water splitting. *Adv Sci* 2022;9:2202417.
- [36] Wang C, Wang X, Gong K, Han DL, Song J, Zhang M. Harnessing the clean energy: phosphorus-alkynyl covalent organic frameworks for photocatalytic hydrogen production. *Int J Hydrogen Energy* 2024;86:293–9.
- [37] Cheng H, Lv H, Cheng J, Wang L, Wu X, Xu H. Rational design of covalent heptazine frameworks with spatially separated redox centers for high-efficiency photocatalytic hydrogen peroxide production. *Adv Mater* 2022;34:2107480.
- [38] Wang C, Qiu TY, Zhao YN, Lang ZL, Li YG, Su ZM, Tan HQ. Phosphorus-alkynyl functionalized covalent triazine/heptazine-based frameworks for high-performance photocatalytic hydrogen peroxide production. *Adv Energy Mater* 2023;13:2301634.
- [39] Wang H, Cheng H, Lv H, Xu H, Wu X, Yang J. Molecular design of two-dimensional covalent heptazine frameworks for photocatalytic overall water splitting under visible light. *J Phys Chem Lett* 2022;13:3949–56.

- [40] Wang C, Li YG, Su ZM, Tan HQ. Design of donor–acceptor type covalent Triazine/heptazine-based frameworks for enhanced photocatalytic water splitting. *Langmuir* 2025;41:33609–17.
- [41] Wang C, Li J, Su ZM. Molecular engineering of metal cluster-based covalent triazine/heptazine frameworks for boosting photocatalytic water splitting. *Int J Hydrogen Energy* 2025;179:151686.
- [42] Jeon JP, Kim YJ, Joo SH, Noh HJ, Kwak SK, Baek JB. Benzotri thiophene-based covalent organic framework photocatalysts with controlled conjugation of building blocks for charge stabilization. *Angew Chem Int Ed* 2023;62:e202217416.
- [43] Zhou E, Wang F, Zhang X, Hui Y, Wang Y. Cyanide-based covalent organic frameworks for enhanced overall photocatalytic hydrogen peroxide production. *Angew Chem Int Ed* 2024;63:e202400999.
- [44] Chakraborty A, Alam A, Pal U, Sinha A, Das S, Saha-Dasgupta T, Pachfule P. Enhancing photocatalytic hydrogen peroxide generation by tuning hydrazone linkage density in covalent organic frameworks. *Nat Commun* 2025;16:503.
- [45] Kresse G, Hafner J. *Ab initio* molecular dynamics for liquid metals. *Phys Rev B Condens Matter* 1994;47:558–61.
- [46] Perdew JP, Burke K, Ernzerhof M. Generalized gradient approximation made simple. *Phys Rev Lett* 1996;77:3865–8.
- [47] Perdew JP, Yue W. Accurate and simple density functional for the electronic exchange energy: generalized gradient approximation. *Phys Rev B Condens Matter* 1986;33:8800–2.
- [48] Blochl PE. Projector augmented-wave method. *Phys Rev B Condens Matter* 1994;50:17953–79.
- [49] Paier J, Marsman M, Hummer K, Kresse G, Gerber IC, Ángyán JG. Screened hybrid density functionals applied to solids. *J Chem Phys* 2006;124:154709.
- [50] Monkhorst HJ, Pack JD. Special points for Brillouin-zone integrations. *Phys Rev B: Solid State* 1976;13:5188–92.
- [51] Wang C, Zhao YN, Lang ZL, Li YG, Su ZM, Tan HQ. Tunable covalent benzoheterocyclic rings constructed using two-dimensional conjugated polymers for visible-light-driven water splitting. *Nanoscale* 2023;15:18883–90.
- [52] Grimme S, Antony J, Ehrlich S, Krieg H. A consistent and accurate *ab initio* parametrization of density functional dispersion correction (DFT-D) for the 94 elements H–Pu. *J Chem Phys* 2010;132:154104.
- [53] Nose S. A unified formulation of the constant temperature molecular dynamics methods. *J Chem Phys* 1984;81:511–9.
- [54] Skúladson E, Karlberg GS, Rossmeisl J, Bligaard T, Greeley J, Jónsson H, Nørskov JK. Density functional theory calculations for the hydrogen evolution reaction in an electrochemical double layer on the Pt(111) electrode. *Phys Chem Chem Phys* 2007;9:3241–50.
- [55] Nørskov JK, Rossmeisl J, Logadottir A, Lindqvist L, Kitchin JR, Bligaard T, Jónsson H. Origin of the overpotential for oxygen reduction at a fuel-cell cathode. *J Phys Chem B* 2004;108:17886–92.
- [56] Wang L, Wan Y, Ding Y, Wu S, Zhang Y, Zhang X, Zhang G, Xiong Y, Wu X, Yang J, Xu H. Conjugated microporous polymer nanosheets for overall water splitting using visible light. *Adv Mater* 2017;29:1702428.
- [57] Ontiveros D, Viñes F, Sousa C. Exploring the photoactive properties of promising MXenes for water splitting. *J Mater Chem A* 2025;13:3302–16.
- [58] Bardeen J, Shockley W. Deformation potentials and mobilities in non-polar crystals. *Phys Rev* 1950;80:72–80.
- [59] Qiao M, Liu J, Wang Y, Li Y, Chen Z. PdSeO₃ monolayer: promising inorganic 2D photocatalyst for direct overall water splitting without using sacrificial reagents and cocatalysts. *J Am Chem Soc* 2018;140:12256–62.
- [60] Qin C, Wu X, Tang L, Chen X, Li M, Mou Y, Su B, Wang S, Feng C, Liu J, Yuan X, Zhao Y, Wang H. Dual donor–acceptor covalent organic frameworks for hydrogen peroxide photosynthesis. *Nat Commun* 2023;14:5238.
- [61] Fu CF, Sun J, Luo Q, Li X, Hu W, Yang J. Intrinsic electric fields in two-dimensional materials boost the solar-to-hydrogen efficiency for photocatalytic water splitting. *Nano Lett* 2018;18:6312–7.